Supporting Information for

Achieving Extremely Concentrated Aqueous Dispersions of Graphene Flakes and Catalytically Efficient Graphene-Metal Nanoparticle Hybrids with Flavin Mononucleotide as a High-Performance Stabilizer

M. Ayán-Varela[a], J. I. Paredes[a], L. Guardia[a], S. Villar-Rodil[a]*, J. M. Munuera[a], M. Díaz-González[b], C. Fernández-Sánchez[b], A. Martínez-Alonso[a], J. M. D. Tascón[a]

[a]Instituto Nacional del Carbón, INCAR-CSIC, Apartado 73, 33080 Oviedo, Spain

[b]Instituto de Microelectrónica de Barcelona, IMB-CNM (CSIC), Campus UAB, 08193 Bellaterra, Barcelona, Spain

*E-mail address: silvia@incar.csic.es

S1. Characterization of the starting graphite

The elemental analyses of C, H, O, N and S were carried out in a LECO Truspec Micro CHNS microanalysis apparatus with a LECO Truspec Micro O accessory for O analysis. Field emission scanning electron microscopy (FE-SEM) images were acquired on a Quanta FEG 650 system (FEI Company) operated at 25 kV.

The graphite yielded 99.1 wt. % C, 0.01 wt. % H, 0.22 wt. % N, and 0.06 wt. % O. The ash content was 0.06 wt. %. Fig. S1 displays field emission scanning electron microscopy (FE-SEM) images of the starting graphite powder. The typical lateral size of its particles is ~50-150 μm.

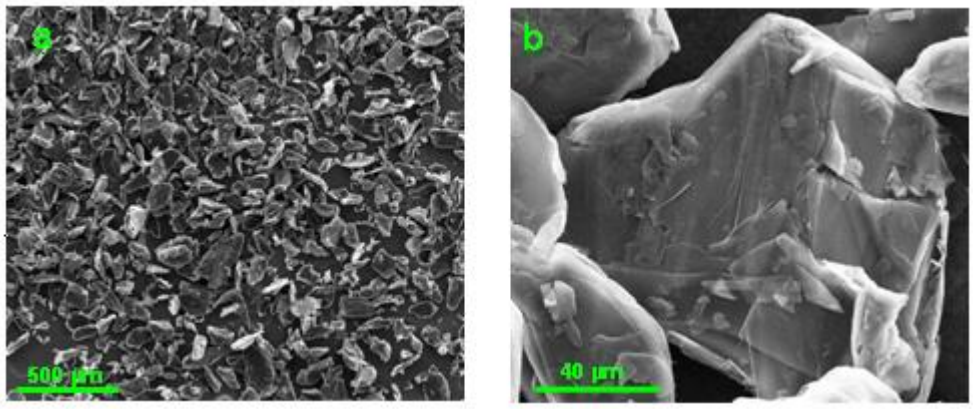

Figure S1. FE-SEM images of the starting graphite powder.

S2. Detailed characterization of the aqueous graphene dispersion stabilized by FMNS

Fig. S2 shows a representative transmission electron microscopy (TEM) image of FMNS-stabilized suspension deposited onto a copper grid covered with a carbon film. A large number of thin lamellar objects with lateral dimensions of a few hundreds of nanometers were observed, providing direct evidence of successful exfoliation of the

graphite particles in the FMNS-water system. This point was further confirmed by atomic force microsocpy (AFM) imaging of the suspensions after being cast onto SiO_2/Si substrates. Large-scale images (e.g., Fig. S2b) revealed a high density of flakes with irregular polygonal shapes and typical lateral sizes in the 100-500 nm range, although objects as long as about 1 μm were also relatively frequent (Fig. S2c). Detailed inspection of the sheets (e.g., Fig. S2d and its corresponding phase image in e) revealed the sheets to be usually decorated with ensembles of discrete particles 10-20 nm wide and about 1 nm high.

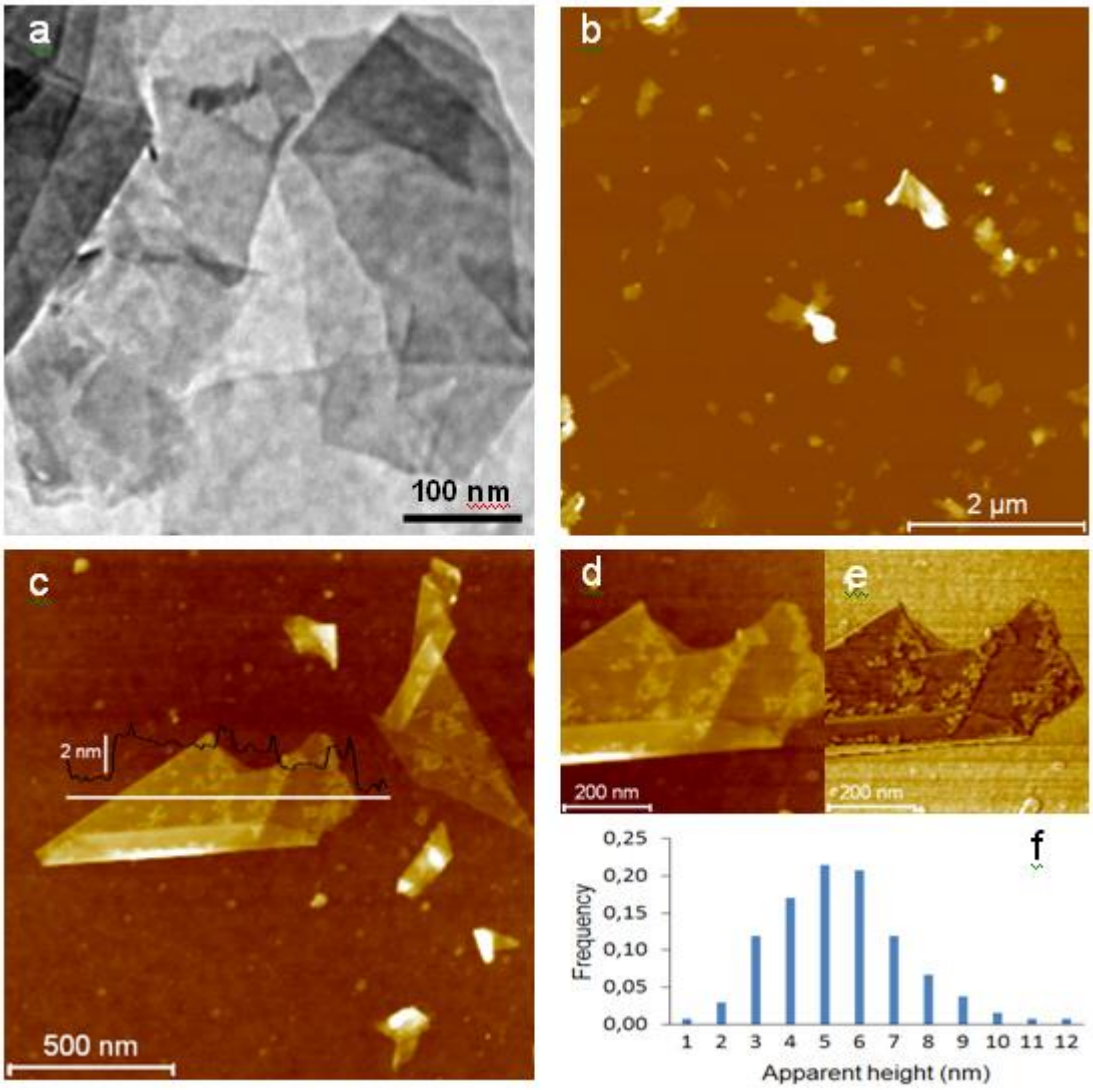

Figure S2. Microscopic characterization of the 0.3 mg mL^{-1} aqueous graphene dispersion stabilized with FMNS: **(a)** TEM image of graphene sheets. **(b)** Tapping mode

AFM height image of the graphene sheets deposited onto Si/SiO_2 substrate. **(c)** Detailed AFM height image and line profile (black trace) of a graphene sheet. The line profile is taken from the white line. **(d)** Magnification of the height image in **(c)**, and **(e)** corresponding phase image. **(f)** Histogram showing the distribution of apparent flake thickness measured on ~140 objects from the AFM images.

We ascribe such particles to some aggregates of the FMNS molecules that were left behind on the flake surface after the dispersions were drop-cast onto the SiO_2/Si substrate and allowed to dry. Indeed, flakes deposited from dispersions that had not been subjected to the purification process and therefore contained much larger amounts of FMNS were seen to be covered (as well as the SiO_2/Si substrate itself) by relatively thick layers of material that has to be attributed to the amphiphilic stabilizer.

Line profiles taken along the exfoliated sheets from the AFM images (an example is shown overlaid on the image of Fig. S2c) allowed determining their apparent thickness. Statistical analysis (Fig. S2f) indicated that such apparent thickness was between 3 and 8 nm for ~90% of the sheets. However, as recently discussed by Paton et al. for surfactant-exfoliated graphene dispersions, inferring the actual thickness (number of monolayers) of the sheets from the AFM measurements is not straightforward and requires some care.[1] Similar to the case of the mentioned authors, we observed the AFM-derived step heights within individual exfoliated sheets to be proportional to ~0.9-1.0 nm, suggesting that every monolayer in a given sheet contributes with that amount to the apparent thickness as measured by this technique. Furthermore, because the adsorbed FMNS aggregates were about 1 nm high, it is reasonable to assume that the measured apparent thickness of the sheets includes a contribution of ~1 nm from the aggregates located between the sheet and the SiO_2/Si substrate.[1] Consequently, a

measured apparent sheet thickness of ~2 nm would correspond to single-layer graphene, and every monolayer that is added to the sheet would increase its apparent thickness by roughly 1 nm. Fig. S3 shows a histogram of the number of graphene monolayers per graphene flake obtained on the basis of such considerations, which reveals that about 75% of them comprised five or less monolayers; i.e., mostly few-layer graphene sheets were produced in the exfoliation and stabilization of graphite using FMNS. This result is comparable to those obtained using other efficient dispersants for graphene.[2-9]

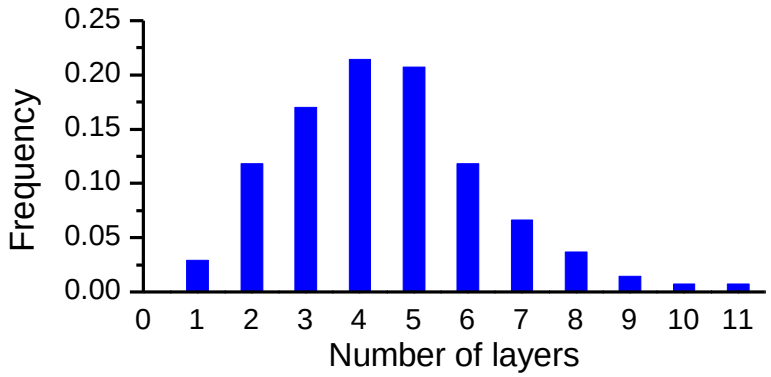

Figure S3. Histogram showing the distribution of the number of monolayers of the graphene flakes measured on ~140 objects from the AFM images.

Fig. S4 shows a typical attenuated total reflection Fourier transformed infrared (ATR-FTIR) spectrum of free-standing paper-like graphene films prepared by vacuum filtration of the corresponding FMNS-stabilized graphene dispersions. The recorded spectra were essentially featureless and therefore consistent with those characteristic of graphene materials with very low or no content of functional groups.[2,10] Furthermore, there was no apparent indication of bands that could be associated to specific molecular groups of FMNS (in particular, in the 1500-1800 cm^{-1} range),[11] suggesting once again

that the exfoliated graphene sheets were colloidally stabilized by a relatively low amount of this amphiphile.

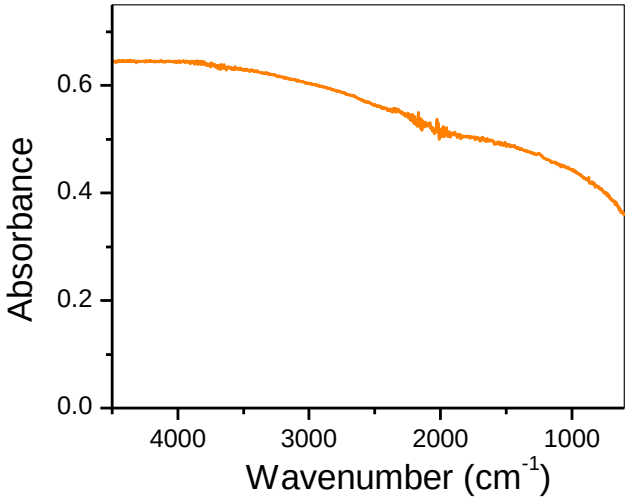

Figure S4. ATR-FTIR of the dried dispersion.

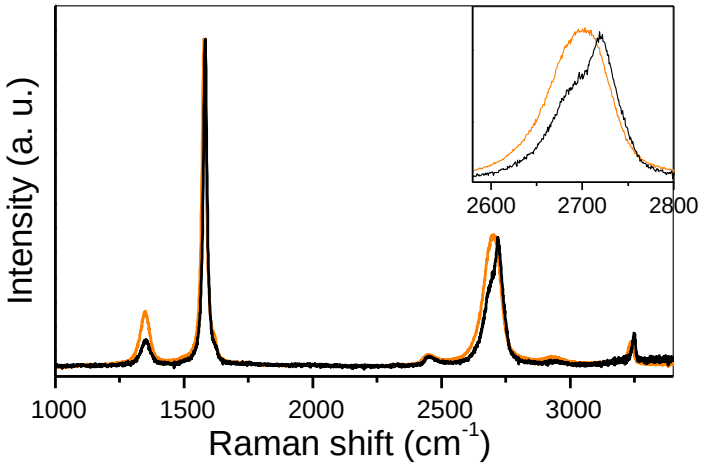

Figure S5. Raman spectrum of the graphene dispersion stabilized with FMNS (orange line) and the bulk, starting graphite (black line). The inset is an enlargement of the 2D band spectral region.

Raman spectroscopy provided evidence that the exfoliated flakes were of a high structural quality. A representative spectrum of the graphene sample is shown in Fig. S5

(orange plot), which is dominated in its first-order region (1100-1800 cm^{-1}) by the well-known G band characteristic of graphitic materials, located at ~1582 cm^{-1}.[12,13] By contrast, the defect-related D band (~1348 cm^{-1}) was rather weak, leading to an integrated intensity ratio of the D and G bands (I_D/I_G ratio) of about 0.17. In comparison, the I_D/I_G ratio of the starting graphite powder (Raman spectrum shown as the black plot in Fig. S5) was ~0.07. This result is comparable to, or even lower than, those of other surfactant-stabilized graphene samples and clearly points to the generation of exfoliated sheets with low defect content.[1,3,4,9,14-16] We believe that the finite value of I_D/I_G for our FMNS-stabilized graphene samples arises mostly, if not entirely, from the non-negligible fraction of edges present in the sheets, which are of relatively small size (typically 100-500 nm; see Fig. S2), and not from defects on their basal plane. Indeed, previous work on the sonication-assisted exfoliation and dispersion of graphite in water in the presence of a large number of surfactants indicated that such a process does not introduce any significant amount of structural defects on the basal plane of the resulting graphene sheets.[3] Furthermore, in addition to the D and G bands, the first-order Raman spectrum of our samples included an additional, very weak peak (D´ band) as a shoulder on the high wavenumber side of the G band (~1620 cm^{-1}), which is also a defect-related peak.[1,17] It has been demonstrated that the $I_D/I_{D'}$ ratio provides information on the nature of the defects present in graphite/graphene.[17] In our case, such a ratio typically amounted to ~5, suggesting that the structural disorder of the FMNS-stabilized sheets was dominated by their graphitic edges, as expected. Significantly, the same $I_D/I_{D'}$ ratio was measured for the starting graphite powder, which indicates that the exfoliation process did not introduce new types of defect on the sheets. The second-order Raman spectrum of both the starting graphite and the FMNS-stabilized graphene flakes comprised, most notably, the 2D (or G´) band located at

about 2700 cm^{-1} (Fig. S5). The shape and position of this band is known to depend on the number of layers and stacking order of graphene materials.[12,13,18] The 2D band is markedly asymmetrical for the starting graphite powder, but appears more symmetrical and down-shifted for the FMNS-exfoliated material (see inset to Fig. S5), which is consistent with the presence of few-layer graphene,[3,4,10,14,18 19] and in turn is in agreement with the AFM results.

S3. Cyclic voltammograms of pure FMNS and pure riboflavin

Several control experiments were made to provide some evidence that the electrochemical response detected from our FMNS-stabilized graphene flakes is really due to FMNS. Based on the FMNS/graphene mass ratio (~0.04) of graphene dispersions determined by XPS (see main text), when the mass of graphene deposited on the GCE is 1.2 μg, the amount of FMNS immobilized on the electrode surface should be about 0.05 μg. We tried to deposit the same amount of pure FMNS without graphene on the GCE surface and compare with the results for FMNS-stabilized graphene flakes to check if the electrochemical response was similar. Adsorption of FMNS on the GCE surface could not be achieved by different strategies (physical adsorption, electrodeposition). Fig. S6a shows the cyclic voltamogram of FMNS in solution with unmodified (dashed line) and graphene modified GCE (solid line). The half-wave potential (-0.5 V vs. Ag/AgCl) of the process is in good agreement with that obtained for FMNS-stabilized graphene films. By contrast, the less water-soluble riboflavin could be deposited in the same amount as in our measurements of the FMNS-stabilized graphene films (~0.05 μg). The response was also qualitatively similar to that of our FMNS-stabilized graphene films, although lower in intensity (see Fig. S6b). This must be due to the fact that, even if we deposit the same amount of riboflavin as that in the FMNS-stabilized graphene films, the exposed surface area of the GCE will be much smaller than that of

the graphene flakes. As a result, there is much more surface for FMNS adsorption on graphene than for adsorption of riboflavin on GCE. As riboflavin has some solubility in water, some of the riboflavin molecules not directly adsorbed on the electrode surface will be lost to the aqueous medium and thus the electrochemical signal will decrease.

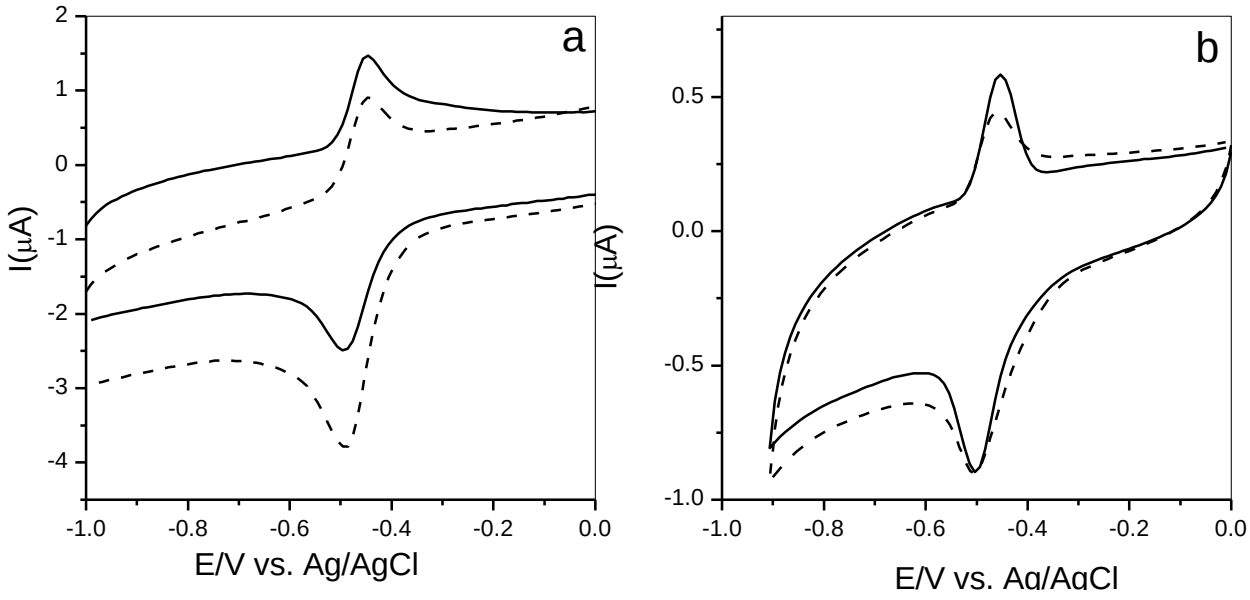

Figure S6.Cyclic voltammograms of **(a)** 0.03 mg L^{-1} FMNS solution in PBS, pH 7.4 with an unmodified GCE (dashed line) and on a graphene (1.2 μg) -modified GCE (solid line); **(b)** 0.05 μg riboflavin deposited on unmodified GCE (dashed line) and on a graphene-modified GCE (solid line).

S4. Reusability of graphene-metal NP hybrids in the catalytic reduction of *p*-nitrophenol (*p*-NP) to *p*-aminophenol (*p*-AP) with $NaBH_4$

The reusability of the graphene-metal NP hybrids was tested by repeating the reduction reaction several times, adding sequentially a given amount of substrate to the colloidal

suspension of the graphene-metal NP hybrid containing an excess amount of $NaBH_4$. Figure S7 shows the results of 8 cycles for the reaction with graphene-Pd NP hybrid. As can be seen, the TOF decreases to ~75 % of its initial value after 8 cycles. The results were similar for the rest of the graphene-metal NP hybrids and are not shown to avoid repetition.

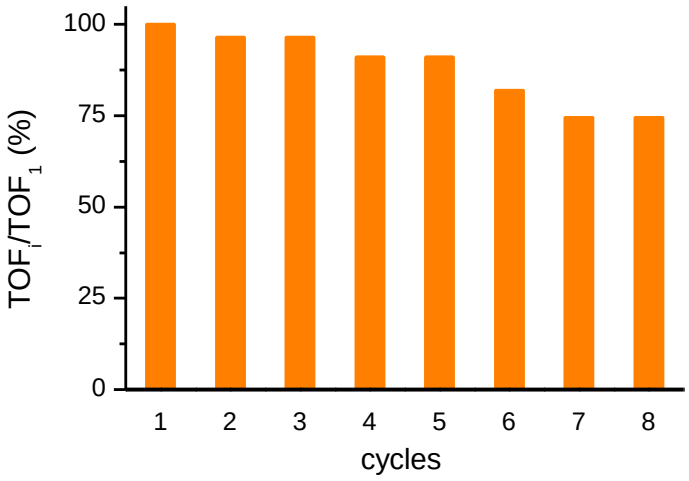

Figure S7. Reusability experiments of graphene-Pd NP hybrid in the catalytic reduction of *p*-NP to *p*-NA. TOF_1 is the TOF for the first cycle and TOF_i stands for the TOF of the cycle number i. The same amount of [*p*-NP] (0.6 mM) was added in each consecutive cycle.

S5. Optimization of the amount of graphene-metal NP hybrid deposited on the GCE to perform the O_2 electroreduction studies

The amount of graphene-metal NP hybrids deposited on the GCEs to perform the O_2 electroreduction study was optimized by performing preliminary studies with serial dilutions of the hybrids in the presence of different concentrations of O_2. As seen in Figure S8 for the graphene-Pt NP hybrid, the modification of the electrode with

amounts of graphene-metal NP hybrids higher than 0.6 μg did not improve the catalytic current. An analogous result was obtained for graphene-Pd NP hybrids, which is not shown to avoid repetition.

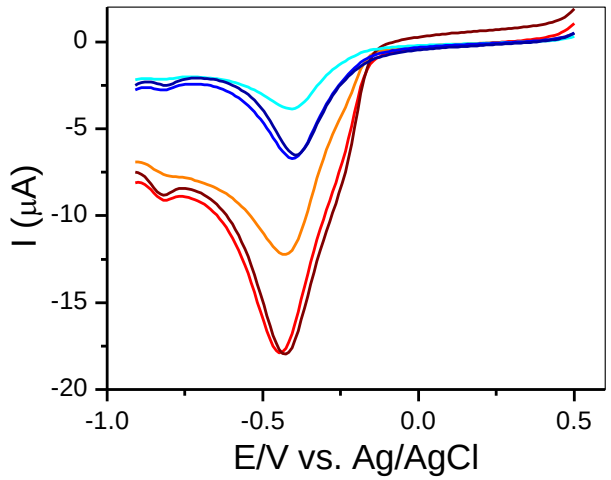

Figure S8. Linear-scan voltammograms of O_2 reduction at electrodes modified with the graphene-Pt NP hybrid in O_2-saturated 0.2 M NaOH solution. The concentration of O_2 and the total mass of deposited graphene were: $[O_2]$ =1 mg L^{-1}, 0.3 μg hybrid (cyan trace); $[O_2]$ =1 mg L^{-1}, 0.6 μg hybrid (blue trace); $[O_2]$ =1 mg L^{-1}, 1.2 μg hybrid (navy blue trace); $[O_2]$ =7.7 mg L^{-1}, 0.3 μg hybrid (orange trace); $[O_2]$ =7.7 mg L^{-1}, 0.6 μg hybrid (red trace); $[O_2]$ =7.7 mg L^{-1}, 1.2 μg hybrid (wine trace). Scan rate: 50 mV s^{-1}.

References

[1] Paton, K. R.; Varrla, E.; Backes, C.; Smith, R. J.; Khan, U.; O'Neil, A.; Boland, C.; Lotya, M.; Istrate, O. M.; King, P.; Higgins, T.; Barwich, S.; May, P.; Puczkarski, P.; Ahmed, I.; Moebius, M.; Pettersson, H.; Long, E.; Coelho, J.; O'Brien, S. E.; McGuire, E. K.; Mendoza Sanchez, B.; Duesberg, G. S.; McEvoy, N.; Pennycook, T. J.; Downing, C.; Crossley, A.; Nicolosi, V.; Coleman, J. N. Scalable Production of Large Quantities

of Defect-Free Few-Layer Graphene by Shear Exfoliation in Liquids. *Nature Mater.* **2014**, *13*, 624-630.

[2] Lotya, M.; Hernandez, Y.; King, P.J.; Smith, R.J.; Nicolosi, V.; Karlsson, L.S.; Blighe, F.M.; De, S.; Wang, Z.; McGovern, I.T.; Duesberg, G.S.; Coleman, J.N. Liquid Phase Production of Graphene by Exfoliation of Graphite in Surfactant/Water Solutions. *J. Am. Chem. Soc.* **2009**, *131*, 3611-3620.

[3] Guardia, L.; Fernández-Merino, M.J.; Paredes, J.I.; Solís-Fernández, P.; Villar-Rodil, S.; Martínez-Alonso, A.; Tascón, J.M.D. High-Throughput Production of Pristine Graphene in an Aqueous Dispersion Assisted by Non-Ionic Surfactants *Carbon* **2011**, *49*, 1653-1662.

[4] Sun, Z.; Masa, J.; Liu, Z.; Schuhmann, W.; Muhler, M. Highly Concentrated Aqueous Dispersions of Graphene Exfoliated by Sodium Taurodeoxycholate: Dispersion Behavior and Potential Application as a Catalyst Support for the Oxygen-Reduction Reaction. *Chem. Eur. J.* **2012**, *18*, 6972-6978.

[5] Wang, Z.; Liu, J.; Wang, W.; Chen, H.; Liu, Z.; Yu, Q.; Zeng, H; Sun, L. Aqueous Phase Preparation of Graphene with Low Defect Density and Adjustable Layers. *Chem. Commun.* **2013**, *49*, 10835-10837.

[6] Sun, Z.; Vivekananthan, J.; Guschin, D.A.; Huang, X.; Kuznetsov, V.; Ebbinghaus, P.; Sarfraz, A.; Muhler, M.; Schuhmann, W. High-Concentration Graphene Dispersions with Minimal Stabilizer: A Scaffold for Enzyme Immobilization for Glucose Oxidation. *Chem. Eur. J.* **2014**, *20*, 5752-5761.

[7] An, X.; Simmons, T.; Shah, R.; Wolfe, C.; Lewis, K.M.; Washington, M.; Nayak, S.K.; Talapatra, S.; Kar, S. Stable Aqueous Dispersions of Noncovalently

Functionalized Graphene from Graphite and their Multifunctional High-Performance Applications. *Nano Lett.* **2010**, *10*, 4295-4301.

[8] Sampath, S.; Basuray, A.N.; Hartlieb, K.J.; Aytun, T.; Stupp, S.I.; Stoddart, J.F. Direct Exfoliation of Graphite to Graphene in Aqueous Media with Diazaperopyrenium Dications. *Adv. Mater.* **2013**, *25*, 2740-2745.

[9] Zhang, L.; Zhang, Z.; He, C.; Dai, L.; Liu, J., Wang L. Rationally Designed Surfactants for Few-Layered Graphene Exfoliation: Ionic Groups Attached to Electron-Deficient π-Conjugated Unit through Alkyl Spacers. ACS Nano **2014**, *8*, 6663-6670.

[10] De, S.; King, P.J.; Lotya, M.; O´Neill, A.; Doherty, E.M.; Hernandez, Y.; Duesberg, G.S.; Coleman, J.N. Flexible, Transparent, Conducting Films of Randomly Stacked Graphene from Surfactant-Stabilized, Oxide-Free Graphene Dispersions. *Small* **2010**, *6*, 458-464.

[11] Ariga, K.; Kamino, A.; Koyano, H.; Kunitake, T. Recognition of Aqueous Flavin Mononucleotide on the Surface of Binary Monolayers of Guanidinium and Melamine Amphiphiles. *J. Mater. Chem.* **1997**, *7*, 1155-1161.

[12] Malard, L.M.; Pimenta, M.A.; Dresselhaus, G.; Dresselhaus, M.S. Raman Spectroscopy in Graphene. *Phys. Rep.* **2009**, *473*, 51-87.

[13] Ferrari, A.C.; Basko, D.M. Raman Spectroscopy as a Versatile Tool for Studying the Properties of Graphene. *Nat. Nanotechnol.* **2013**, *8*, 235-246.

[14] Buzaglo, M.; Shtein, M.: Kober, S.: Lovrinčić, R.: Vilan, A.; Regev, O. Critical Parameters in Exfoliating Graphite into Graphene. *Phys. Chem. Chem. Phys.* **2013**, *15*, 4428-4435.

[15] Bourlinos, A.B.; Georgakilas, V.; Zboril, R.; Steriotis, T.A.; Stubos, A.K.; Trapalis, C. Aqueous-Phase Exfoliation of Graphite in the Presence of Polyvinylpyrrolidone for

the Production of Water-Soluble Graphenes. *Solid State Commun.*, **2009**, *149*, 2172-2176.

[16] Notley, S.M. Highly Concentrated Suspensions of Graphene through Ultrasonic Exfoliation with Continuous Surfactant Addition. *Langmuir* **2012**, *28*, 14110-14113.

[17] Eckmann, A.; Felten, A.; Mishchenko, A.; Britnell, L.; Krupke, R.; Novoselov, K.S.; Casiraghi C. Probing the Nature of Defects in Graphene by Raman Spectroscopy. *Nano Lett.* **2012**, *12*, 3925-3930.

[18] Hao, Y.; Wang, Y.; Wang, L.; Ni, Z.; Wang, Z.; Wang, R.; Koo, C.K.; Shen, Z.; Thong, J.T.L. Probing Layer Number and Stacking Order of Few-Layer Graphene by Raman Spectroscopy. *Small* **2010**, *6*, 195-200.

[19] Khan, U.; O´Neill, A.; Lotya, M.; De, S.; Coleman, J.N. High-Concentration Solvent Exfoliation of Graphene. *Small* **2010**, *6*, 864-871.